Soft Magnetic Material Degradation due to Manufacturing Process: A Comparison of Measurements and Numerical Simulations

G. von Pfingsten, S. Steentjes, A. Thul, T. Herold, and K. Hameyer, *Senior Member IEEE*
Institute of Electrical Machines (IEM), RWTH Aachen University, Germany
Email: georg.vonpfingsten@iem.rwth-aachen.de

***Abstract*—Iron losses are one major origin of losses in highly utilized electrical machines. This work presents how iron losses can be modeled including material deterioration due to manufacturing processes. The obtained model is used to improve the machine design process and understand currently used building factors. These factors are state-of–art in describing iron-loss increase by processing of electrical steel. Aim of this work is to understand the origins of these building factors and give the possibility to the machine designer to estimate the influence of magnetic circuit design and soft magnetic material choice on the machines iron losses and therefore efficiency and power density. The electrical steel is characterized by measurements in the Single-Sheet-Tester with various numbers of cutting edges. Finally, comparisons of measurements and numerical simulations of an 80 kW interior permanent magnet machine are given.**

I. Introduction

THE losses are a major design factor for designing highly utilized electrical machines. Since the maximal heat dissipation is limited by the cooling system, the knowledge and predictability of the machines losses is crucial for designing new machines and improving existing machine designs. For highly utilized machines with high electrical operating frequencies the iron losses make a large share of the overall losses. The electrical steel in machines is subject to several processing steps. These steps are usually cutting the steel and stacking it to a laminated core. The stator core is then fixed in the housing of the machine and the rotor core on the rotor shaft. Different techniques could be used for every of these steps.

The steel laminations of the studied machine are dissected by laser cutting. The laminations are stacked to the core using a bonding varnish.

The deteriorating effect of the cutting process on the magnetic properties of the material close to the cut edge is well known [1]–[3], [6]–[8]. In comparison to guillotine cutting where the sheet experiences plastic deformation and the mechanical energy supplied to the material is absorbed by the lattice through a shift of the neighboring layers, laser cutting induces bi-axial thermal stresses due to heat-up of the sample [3]. It depends hence basically on the geometry of the lamination, in particular on the lamination thickness d, as well as on structural elements such as the grain size. Microstructural defects appear, which operate as pinning sites for domain walls. This results in a local modification of the microstructure (dislocations, internal stresses, grain morphology) influencing both the magnetic and mechanical properties of the steel [1], [2].

Improved estimation of iron losses occurring in stator and rotor core of machines is essential for the design of highly efficient electrical drives [4]. Therefore, the relationship between the deterioration of the magnetic properties, alloy type, material thickness, rolling direction, and other parameters like operating range of magnetic flux density and frequency needs to be investigated and included in the design process of electrical machines.

This paper presents a quantitative analysis of the influence of lamination processing for non-oriented electrical steels custom-made for traction drives used in automotive applications. The analysis is performed over a wide range of frequency f to study the influence of increasing eddy currents on the cut edge effect and to reproduce the operating range of electrical machines in the envisaged applications. On that account, material characteristics are measured for samples with different ratios of cut edge length vs. overall lamination volume, i.e., varying the amount of cut surface related to the material volume. A number of single sheet tester samples of 120 mm by 120 mm are cut in smaller stripes by CO_2 laser cutting resulting in different sample sets with additional laser cut edges. The total width remains 120 mm. In order to study the impact on the magnetization behavior, quasi-static measurements with negligible amount of eddy current disturbance are conducted. Based on these measured data the impact on the different loss terms in the IEM-formula [4], is analyzed in detail. A differentiated understanding of the influences can be obtained, and thus the sensitivity of the various terms in terms of the processing of steel laminations be evaluated. This is important for the design of electrical machines, but also for the development of custom-made electrical steels.

Subsequently, a permanent magnet synchronous machine is simulated and machine measurements are conducted to study the efficiency of the proposed iron-loss calculation procedure. Therewith an improved understanding of the commonly used empirical building factor [11], [12] and their origin is possible.

II. Characterization of the Electrical Steel

The 3.2 wt% silicon steel which is used for the laminations of the machine is cut by a CO_2 laser. This grade is optimized in order to have lower deterioration of magnetic properties of the laminations. Low losses at high frequencies and guaranteed yield strength in rolling direction for room temperature are other advantages of this grade.

978-1-4799-5162-8/14/$31.00 ©2014 IEEE

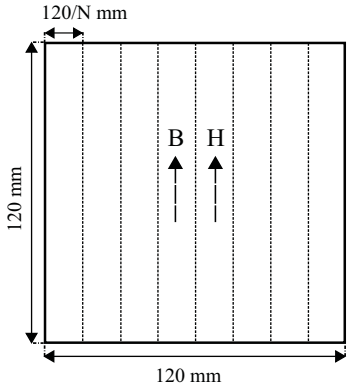

Fig. 1: SST sample sets of the electric steel. N equals the number of samples.

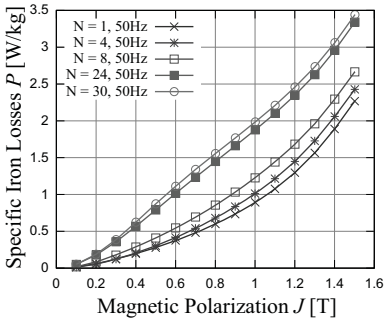

Fig. 2: Measured data for the various sample sets at 50 Hz.

In order to quantify the influence of the CO_2 laser cutting process on the properties of the electrical steel, different single-sheet-tester (SST) sample sets with different amount of cut edges are cut using the same laser process parameters. The SST uses sample sizes of 120 x 120 mm. To obtain samples in this dimension, N multiple smaller strips with a length of 120 mm and a width of $\frac{120\,\mathrm{mm}}{N}$ are combined to one sample (Fig. 1).

Measurements are performed utilizing the field-metric method under sinusoidal magnetic flux densities up to high amplitudes of 1.8 T at excitation frequencies of 10 , 50 , 400 , 700 , and 1 kHz. Quasi-static characteristics are identified by point-by-point dc-measurements, i.e., quasi-constant current, using a flux-meter.

Fig. 2 presents measured data at 50 Hz for the various sample sets. It is apparent that once the number of cut edges is increased, the iron losses significantly increase. This increase could be traced back to an increased hysteresis loss contribution due to additional pinning sites [1]. It is seen that a decreasing sample size, i.e., an increasing proportion of the degraded zone, leads to much higher hysteresis losses.

Using the measured data the impact of cutting on the coefficients of the IEM-formula (1) can be studied:

$$P(\hat{B}, f) = a_1 \hat{B}^{\alpha} f + a_2 \hat{B}^2 f^2 (1 + a_3 \hat{B}^{a_4}) + a_5 (\hat{B} f)^{1.5}, \quad (1)$$

with pure hysteresis, classical eddy current, excess eddy current and saturation losses included as terms with a_1, a_2, a_5 and a_3, a_4. Parameter α is kept constant to 2.0, resulting in best agreements between measured quasi-static hysteresis loss and estimated ones. Assuming that the chemical composition, consequently the specific electrical resistivity, is locally not influenced by the cutting process, the classical induced eddy currents (a_2) are not directly influenced by the cutting technique, only its distribution will (indirectly) be affected by the cut edge properties. This is due to the variation of the local magnetic flux density $J(x)$. Another assumption, that the microstructural characteristics do not alter (just locally near to the cut edge if any) implies a constant excess loss parameter (a_5).

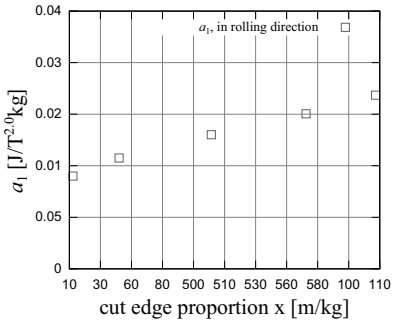

Fig. 3: Parameter a_1 as a function of the cut edge proportion with $\alpha = 2.0$ for CO_2 laser cut sample sets in rolling direction.

Based on this it is assumed that the quasi-static hysteresis losses are most prone to be affected by cutting, corroborated by the behavior of the coercive field $H_c(H)$ and the quasi-static hysteresis loops $J(H)$. Hence, parameter a_1 related to the pure hyteresis loss is adapted to account for the increasing dislocation density for decreasing sample width. Ref. [8] shows that the magnetic property deterioration depends on the cutting strains, defined as $S = A/V$, i.e., the cutting surface $A(\mathrm{m}^2)$ referenced to the volume $V(\mathrm{m}^3)$.

As a first step, parameter a_1 is identified for each sample set using point-by-point dc-measurements allowing to determine a_1 solely [10]. Fig. 3 show the obtained parameters as a function of the amount of the cut edge per sample mass, i.e., the cut edge length l_{cut} related to the weight of the sample m_s, based on the dependence of the magnetic property deterioration on the cutting strains [8]. A linear relation is apparent. This advantageous linear interdependence is exploited to adapt a_1. Given the mathematical description for the iron losses (1), it is proposed to rewrite the hysteresis loss contribution as

$$P_{\mathrm{hy}}(\hat{B}, f, x) = a_1(x) \hat{B}^{\alpha} f, \quad (2)$$

with $\alpha = 2.0$. In this hysteresis loss description, the hysteresis coefficient a_1 has become dependent on the cut edge proportion $x = l_{cut}/m_s$:

$$a_1(x) = a_{1,\mathrm{ref}} + m \cdot (x - x_{\mathrm{ref}}), \quad (3)$$

where m is the gradient of the linear equation, which could be determined by a line of best fit through the estimated a_1-parameters of different sample sets (in this case $a_{1,\mathrm{ref}}$ would be the a_1-axis crossing and x_{ref} identical zero), but also using only two points in the $a_1 - x$ space. Therewith it is possible to calculate the iron-loss in cut sample sets at least from

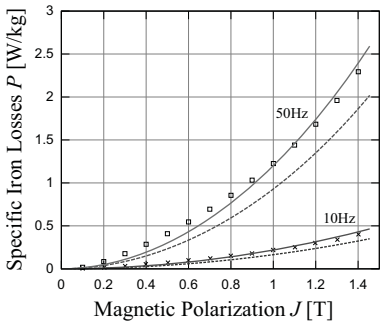

Fig. 4: Comparison of loss-predictions for the eight 15-mm ($N = 8$) wide CO_2 laser cut samples using a_1 of the undivided sample (dotted lines) and the adapted one (straight lines) with measured losses (markers).

any two parameter sets a_1, for instance using the parameter set of undivided sample (120 mm by 120 mm) as a reference ($a_{1,\text{ref}} \equiv a_{1,120\text{x}120}$ and $x_{\text{ref}} = l_{\text{cut},120\text{x}120}/m_{\text{s},120\text{x}120}$) combined with a_1 of any smaller sample set to determine the slope. Using this, parameter a_1 is adapted according to the actual cut edge proportion. The other parameters in the loss description were kept constant, i.e., parameters a_2 to a_5 need to be identified once at the reference sample set following the procedure presented in [10].

Fig. 4 shows resulting loss-predictions for the 15 mm wide CO_2 laser cut sample sets obtained using the linear relation for a_1 as a function of the cut edge length per mass for magnetic flux densities up to 1.5 T and frequencies between 10 Hz and 50 Hz. It is remarkable that the loss predictions using just the adapted a_1, i.e., just modifying the quasi-static hysteresis loss, while leaving the other parameter constant provide a good accordance with the measured ones. This corroborates the assumption that parameter a_1 is most prone to cut edge effects. Higher frequencies are omitted in Fig. 4 for reasons of clarity. For frequencies above 1000 Hz at magnetic flux densities above the knee-point (i.e. 1.2 T) small deviations appear increasing with frequency, clearly related to different non-linear magnetization behavior, which is significantly influenced by the material processing. In order to consider this, parameters a_3 and a_4 describing the non-linear (saturation) losses, need to be adapted. This will be one of the next steps of this research work.

III. Simulation of the Machine

The machine is simulated using the in-house FE-software package *pyMoose* [13]. The measured magnetization curve of the electric steel is used in these simulations.

A. Machine Data

The analyzed machine is an $2p = 8$ pole synchronous machine with V-shaped buried magnets (VPMSM). The 48 stator teeth are each 6.25-mm wide and 35-mm long. The stator back-iron yoke has a radial dimension of 20 mm.

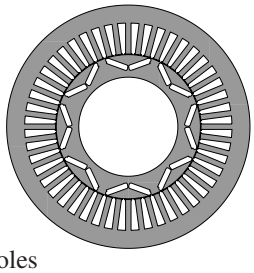

number of poles	8	
nominal speed	3,125	min^{-1}
maximum speed	8,000	min^{-1}
rated power	50	kW
maximum power	80	kW
maximum torque	300	Nm
number of stator teeth	48	
width of stator teeth	6.25	mm
length of stator teeth	35	mm
radial dimension of stator yoke	20	mm
cut edges per mass, stator - teeth	141	$\frac{m}{kg}$
cut edges per mass, stator - yoke	44	$\frac{m}{kg}$
cut edges per mass, stator - average	82	$\frac{m}{kg}$
thickness of 3.5 wt.% electrical steel	0.3	mm

B. FEM modeling of the machine

Detailed two-dimensional FEM-simulations with 180 angular steps per electric period of the studied machine were conducted. The d- and q-axis currents I_d, I_q are varied in 13 steps resulting in a current-plane (Fig. 5).

Single-valued magnetization curves have been used; thereby saturation effects originating from the non-linear material behavior are included. Second-order effects, originating from hysteresis behavior, are neglected. Therefore the FEM simulations are independent of the electric fundamental frequency f_1. This gives the possibility to scale the results by f_1 corresponding to the desired operating speed n. Pure hysteresis (P_hyst), classical eddy current ($P_\text{classical}$), excess (P_excess) and saturation losses (P_sat) in the laminated stator and rotor core are estimated *a posteriori* using the local waveforms of the magnetic flux densities in every element using the extended IEM-formula (4) detailed in [9], [10].

$$P_{Fe} = P_\text{hyst} + P_\text{classical} + P_\text{excess} + P_\text{sat} \tag{4}$$

with the following loss contributions:

$$P_\text{hyst} = a_1 \left(1 + \frac{B_\text{min}}{B_\text{max}} \left(r_\text{hyst} - 1\right)\right) B_\text{max}^{\alpha} f \tag{5}$$

$$P_\text{classical} = a_2 \sum_{n=1}^{\infty} \left(B_\text{n}^2 \left(nf\right)^2\right) \tag{6}$$

$$P_\text{excess} = a_5 \left(1 + \frac{B_\text{min}}{B_\text{max}} (r_\text{excess} - 1)\right) \sum_{n=1}^{\infty} \left(B_\text{n}^{1.5} \left(nf\right)^{1.5}\right) \tag{7}$$

$$P_\text{sat} = a_2 a_3 B_\text{max}^{a_4+2} f^2 \tag{8}$$

B_n is the amplitude of the n-th harmonic component of the magnetic flux density in Tesla (T), n the order of harmonic, f the fundamental frequency in Hertz (Hz), $\alpha, a_1 - a_5$ the material specific parameters and r_hyst, r_excess the rotational loss factors [4] [5].

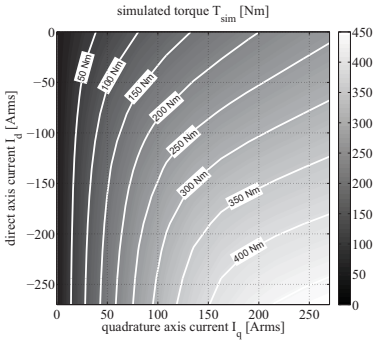

Fig. 5: Simulated torque.

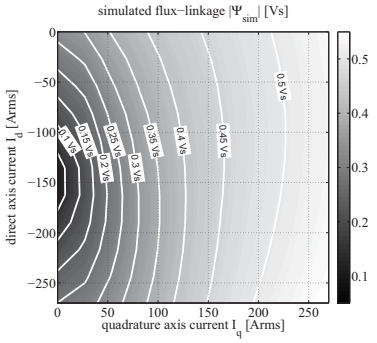

Fig. 6: Simulated flux-linkage.

Combining the material information (loss and non-linear magnetization behavior) with a finite element model and a specific control strategy to incorporate the operation characteristics of the machine is the most sophisticated approach used in this research work. Therefore, specific iron-loss calculation (for a fixed f_1) is done for each finite element. The best operating points of the machine are found by evaluating torque T and flux linkage Ψ over the simulated current plane (Figs. 5 and 6). Valid operating points in means of voltage and current limitation are found from these simulations. In combination with the rotational speed n, the fundamental frequency in every $T-n$-operating point is given and the iron losses are scaled to fit to this frequency. From n in every operating point the frequency $f_1 = n \cdot p$ is calculated.

Figures 7 and 8 show the simulated iron losses at a frequency of 180 Hz ($n = 2700\,\mathrm{min}^{-1}$). It is apparent, that the hysteresis iron losses are linked to the flux in the machine. At $I_\mathrm{d} = -150\,\mathrm{Arms}$ and $I_\mathrm{q} = 0\,\mathrm{Arms}$, where the absolute value flux linkage reaches its minimum, the minimal hysteresis losses are found. Whereas the sum of iron losses show a different dependency on the electric current in the machine, tending to higher iron losses at higher currents.

Figures 8 and 9 show the influence of an increased hysteresis parameter a_1 due to cutting over the simulated $d-q$-current-plane. One can see, that the highest relative loss increase in the simulation is at points with $I_\mathrm{d} > -100\,\mathrm{Arms}$ and $I_\mathrm{q} < 150\,\mathrm{Arms}$. These points correspond to the *Maximum Torque per Ampere* (MTPA) operation of the machine below 200 Nm. At a speed of $2700\,\mathrm{min}^{-1}$ the iron losses are increased by 20 % because of the laser cutting. At higher torque MTPA operating points the flux saturates and the impact of the relative

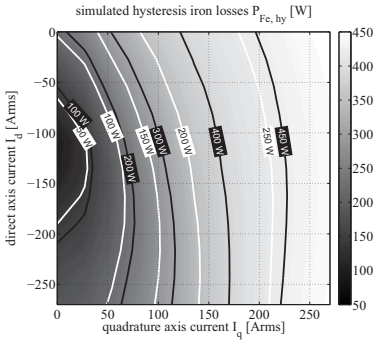

Fig. 7: Simulated hysteresis iron losses with (black lines) and without (white lines) influence of cutting.

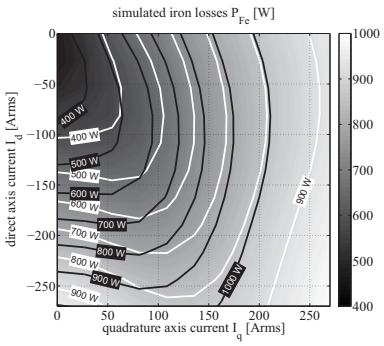

Fig. 8: Simulated iron losses with (black lines) and without (white lines) influence of cutting.

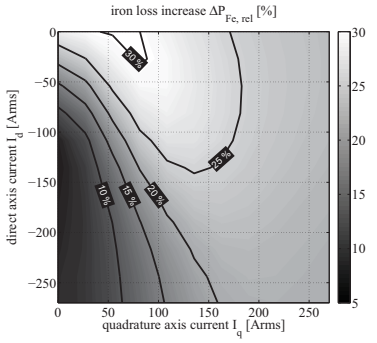

Fig. 9: Simulated relative iron loss increase due to cutting.

increase of hysteresis iron losses is reduced. Whereas the eddy current losses and the saturation losses tend to further increase even at higher saturated operating points. Therefore the relative influence of an increased a_1 is reduced for higher torque values.

IV. Measurements of the Machine

In order to validate the proposed model of deterioration by cutting, measurements of the machines losses are conducted. At first, a measurement series is performed at a constant speed of $2700\,\mathrm{min}^{-1}$ and variation of I_d and I_q. A second measurement series is conducted at variable speed and torque. The measurement equipment used for the measurements is:

- YOKOGAWA WT3000 Precision Power Analyzer - Motor Version

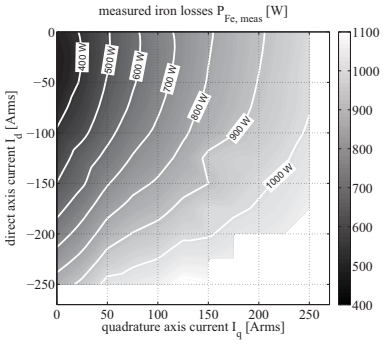

Fig. 10: Measured iron losses.

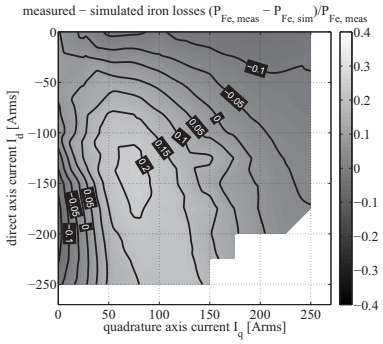

Fig. 11: Relative error of iron loss estimation with cut edges.

- 3 LEM IT 400-s Ultrastab High Precision Current Transducer
- HBM T12 Digital Torque Transducer
- NI PXIe 4353 - Thermocouple Input Module
- 11 Type J Thermocouples
  - 3 in each end winding
  - 5 distributed in different slots

The losses P_v inside the machine are measured as difference of the 3-phase input electrical power P_Σ and the mechanical output power of the machine P_m. The winding temperature varied during the measurements between 80 and 120 °C. With thermocouples in both the end windings and slots, it is possible to identify the change of the winding resistance during the measurement due to different thermal conditions. A reference measurement of the winding resistance was undertaken at room temperature. A temperature coefficient of $\alpha_\mathrm{Cu} = 0.0039\,\mathrm{K}^{-1}$ is used to map the ohmic resistance to the current winding temperature. The ohmic copper losses P_Cu are then calculated using the measured current and the adjusted ohmic resistance. The friction losses P_f are determined using analytical formulae. The friction in the air gap $P_\mathrm{f,\,ag}$ is determined by (9) [14]. l_Fe is the length of the machine and $v_\mathrm{lat,\,rotor}$ the lateral surface speed of the rotor. The friction losses on the two axial face sides of the rotor are described by the the additional term using the pole pitch τ_p.

$$P_\mathrm{f,\,ag} = 3 \cdot D_\mathrm{o,\,rotor} \cdot \left(l_\mathrm{Fe} + 0.8^3 \cdot 0.6 \cdot \tau_\mathrm{p}\right) \cdot v_\mathrm{lat,\,rotor}^2 \qquad (9)$$

The friction losses in the two bearings ($\mathrm{n_b} = 2$) of the machine $P_\mathrm{f,\,b}$ are calculated in (10) [15]. With d_b being the average diameter of the bearing and the coefficient f_0, which is depending of the type of bearing and its operation conditions such as bearing temperature. f_0 was extracted from the online tool of the bearing manufacturer from [16].

$$P_\mathrm{f,\,b} = \mathrm{n_b} \cdot 2\pi \cdot n \cdot 10^{-7} f_0 \cdot (v_\mathrm{b} \cdot n)^{\frac{2}{3}} \cdot d_\mathrm{b}^3 \qquad (10)$$

The iron losses $P_\mathrm{Fe,\,meas}$ are then determined using (11).

$$P_\mathrm{Fe,\,meas} = P_\Sigma - P_\mathrm{Cu} - P_\mathrm{f,\,ag} - P_\mathrm{f,\,b} \qquad (11)$$

A. Measurements at constant speed

The measurements at constant speed are performed to validate the influence of cutting and the iron loss model for different levels of flux densities and flux density harmonics. With variation of I_d and I_q, different flux paths inside the core of the machine are passed by the magnetic flux. Different harmonic effects originating from the stator winding distribution and the arrangement of the permanent magnets in the rotor occur. Therefore, the iron losses are not only depending on the speed of the machine, but also on the value of I_d and I_q. Since in 4 harmonics in every location in the 2D-cross section are regarded, these effects are taken into account by the simulations.

At negative I_d and low I_q currents, a low flux linkage in the machine is reached. However, additional harmonics caused by winding distribution and the stator slotting of the machine lead to higher flux pulsations in the stator teeth. Therefore, higher foucault eddy current losses are to found in this operation mode. The hysteresis iron losses, strongly depending on the flux density inside the core material, is lower at operating points with lower flux linkage.

The iron losses as a result of 11 over I_d and I_q are shown in Fig. 10. Figure 11 shows the relative error of the simulated iron losses $P_\mathrm{Fe,\,sim}$ taking cut edges into account. Without taking cut edges into account the average error is 20.3 % or 163.6 W in absolute values. Taking cut edges into account reduces the average error by 55 % to 9.0 %, or 73.9 W respectively. The maximum error is reduced from 31.2 % to 21.5 % by taking into account the cut edge effect.

B. Measurements - torque-speed maps

To evaluate the iron losses over the normal operation range of the machine, measurements at different speeds are conducted. First, the operating points in the base speed area of the machine are found using MTPA. For higher speeds the flux-linkage limit (and therefore voltage limit) is taken into account. Only operating points inside certain flux-linkage ellipses are valid. It is apparent, that the field-weakening operation starts between a speed of $2700\,\mathrm{min}^{-1}$ and $4000\,\mathrm{min}^{-1}$.

Fig. 12 shows the simulated hysteresis losses over torque and speed. One can see, that in base speed operation, the hysteresis losses rise with speed. They reach the maximum at the points where field weakening is necessary. From there

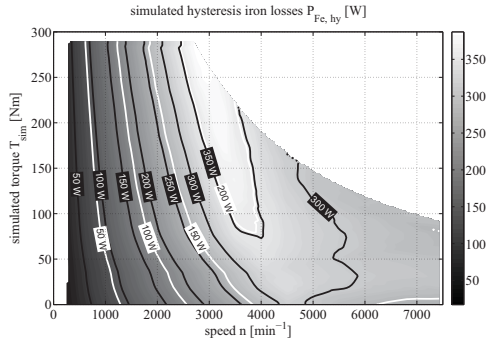

Fig. 12: Simulated hysteresis iron losses without taking cut edges into account vs. speed and torque.

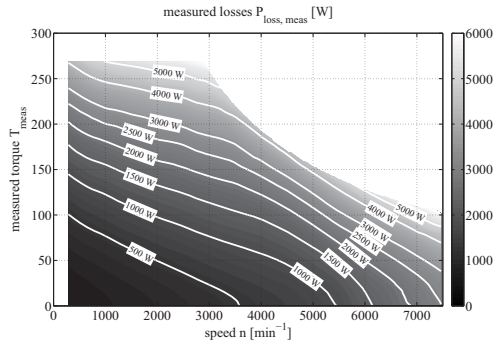

Fig. 13: Measured overall losses vs. speed and torque.

on the hysteresis losses decrease with speed. Modeling the hysteresis losses as cut edge dependent therefore means modeling a loss increase especially in operating points close to field weakening operation.

Fig. 13 shows the measured losses P_{v}. One can see that the highest losses of ca. 6000 W are dissipated at high torque operating points at base speed as well as at maximum speed operation. The iron losses over speed and torque are measured as discussed before and shown in fig. 14. It is apparent, that the iron losses reach their maximum of ca. 4000 W at the operating point with the highest possible torque at the highest speed. As a comparison, the simulated iron losses are shown in Fig. 15. The error of the simulation with losses due to cut edges is shown in Fig. 16. One can see, that at high power operation points the iron loss is underestimated by ca. 500 W. Hence at speeds above $4000\,\mathrm{min}^{-1}$ and torques below 30 Nm the simulation overestimates the iron losses in the machine by up to 250 W. The average error in estimating the iron losses without taking cut edges into account is 220.7 W respectively 32.3 % of the measured iron losses. When taking the cut edges into account by adjusting a_1 according to the SST measurements (i.e. increasing a_1 by 77 % to 0.0276), the average error is reduced to 164.3 W respectively 22.3 %.

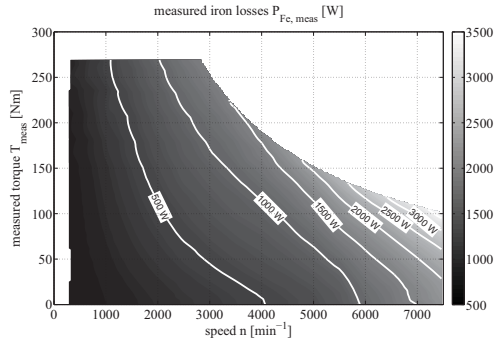

Fig. 14: Measured iron losses vs. speed and torque.

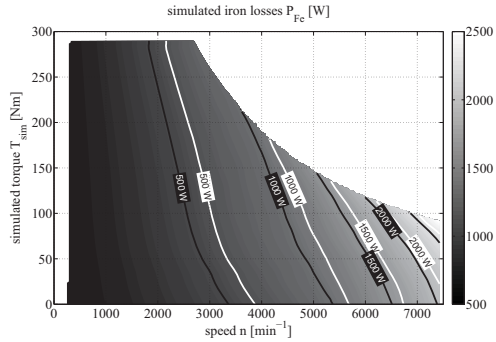

Fig. 15: Simulated iron losses, with cut-edge effect (black lines), without cut-edge effect (white lines).

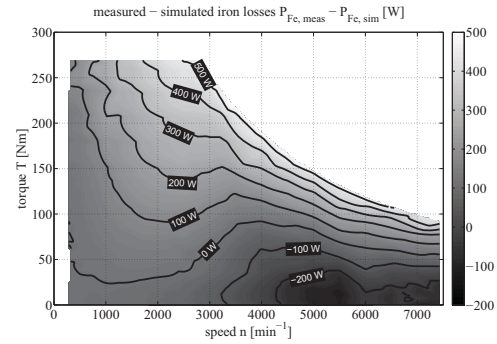

Fig. 16: Simulated vs. measured iron losses taking cut-edges into account.

V. Discussion

Analyzing the difference of the estimated iron losses by measurements (11) and from simulation (4) shows areas of over- und underestimation in the simulation (fig. 16). At speeds above $4000\,\mathrm{min}^{-1}$ and torque values below 50 Nm, an overestimation of the iron losses up to 250 W in the simulation is seen. This effect could be explained by overestimating the friction losses by [14] and [15] in (11), which leads to an underestimation of the iron losses at high speeds from the measurements. Since the rotor excitation is permanent, the friction losses can not be measured with the used test setup.

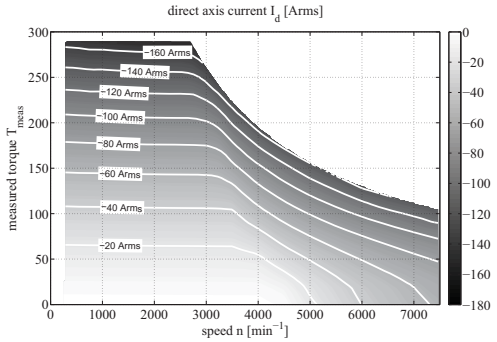

Fig. 17: Direct current vs. speed and torque.

At operating points with high absolute direct axis currents $|I_\mathrm{d}| > 140\,\mathrm{Arms}$ an underestimation of the iron losses by the simulation of ca. 500 W is observed. A possible explanation is, that additional axial flux paths in the core material lead to additional eddy currents in the lamination. Since the machine core was stacked using bonding varnish, inter-laminar short circuit currents are not to be expected. Because the machine is skewed by one stator slot pitch, axial flux path in the rotor and stator cores are possible. A skewed machine generates higher axial flux components and therefore higher eddy current losses [17]. When comparing the estimation error from fig. 16 to the direct axis current (fig. 17) it can be seen, that the highest loss underestimation goes in hand with the highest negative current in the direct axis. Since a high negative d-axis current creates a magnetic field from the stator that opposes the permanent magnet excited field of the rotor. Higher magnetic stray flux emerges. Hence the lamination is not effective for axial flux components, a higher flux and therefore stray flux in axial direction leads to additional eddy current losses as described in [17].

VI. Conclusions

The influence of cut edges on the iron losses occurring in electrical machines is studied. SST Measurements of the magnetic properties of a magnetic steel were conducted. Samples with different amount of cutting edges were prepared and measured. Based on quasi-static measurements effects on the intrinsic magnetization behavior and quasi-static hysteresis loop characteristics are studied without the need to account for dynamic effects due to induced eddy currents. A linear relation between quasi-static hysteresis loop area and cut edge length per mass is found. Subsequently a method to consider the increasing influence of cutting strains with decreasing sample sizes on the pure hysteresis loss is proposed.

The accuracy of the proposed method is underlined comparing measured and predicted losses over a wide frequency range along the rolling direction. The parameters in the model from (4) were found to fit for different amount of cut-edge length per mass. A 80 kW permanent magnet machine with the same electrical steel was measured. The adapted advanced iron loss model from [9], [10] was used to simulate the iron losses in the machine with the influence of cutting. A significant enhancement of the iron loss prediction without any additional building factors was found. Next steps are to analyze the influence of shrink fitting [18] and compressive stress [19]–[21] on the iron losses in the machine.

References

[1] A.J. Moses, N. Derebasi, G. Loisos, and A. Schoppa, “Aspects of the cut-edge effect stress on the power loss and flux density distribution in electrical steel sheets,” *J. Magn. Mag. Mat.*, pp. 690–692, June 2000.

[2] G. Crevecoeur, P. Sergeant, L. Dupre, L. Vandenbossche, and R. Van de Walle, “Local Identification of Magnetic Hysteresis Properties Near Cutting Edges of Electrical Steel Sheets,” *IEEE Trans. on Magn.*, vol. 44, no. 11, pp. 3173–3176, 2008.

[3] R. Siebert, J. Schneider, and E. Beyer, “Laser Cutting and Mechanical Cutting of Electrical Steels and its Effect on the Magnetic Properties,” *IEEE Trans. on Magn.*, vol. 50, no. 4, pp. 1–4, April 2014.

[4] S. Steentjes, M. Leßmann, and K. Hameyer, “Advanced Iron-Loss Calculation as a Basis for Efficiency Imrpovement of Electrical Machines in Automotive Application,” *IEEE Conf. Proc. ESARS*,pp. 1–6, 2012.

[5] G. Bertotti, A. Canova, M. Chiampi, D. Chiarabaglio, F. Fiorillo, and A. Rietto, ”Core loss prediction combining physical models with numerical eld analysis”, *Journal of Magnetism and Magnetic Materials*, vol. 133, pp. 647–650, 2004.

[6] M. Emura, F. J. G. Landgraf, W. Ross, and J. Barreta, “The influence of cutting technique on the magnetic properties of electrical steels,” *J. Magn. Magn. Mat.*, vol. 254, pp. 358-360, 2003.

[7] G. Lu, A. Kotousov, and E. Siores, “Elementary mathematical theory of thermal stresses and fracture during welding and cutting,” *J. Mater. Technol.*, vol. 89, pp. 298–302, 1999.

[8] B. Hribernik, “Influence of cutting strains on the magnetic anisotropy of fully processed silicon steels,“ *J. Mag. Mag. Mat.*, vol. 26, pp.72–74, 1982.

[9] S. Steentjes, G. von Pfingsten, M. Hombitzer and K. Hameyer, ”Iron-Loss Model With Consideration of Minor Loops Applied to FE-Simulations of Electrical Machines,” Magnetics, IEEE Transactions on , vol.49, no.7, pp.3945,3948, July 2013

[10] S. Steentjes, M. Leßmann, K. Hameyer, ”Semi-physical parameter identification for an iron-loss formula allowing loss-separation,” Journal of Applied Physics , vol.113, no.17, pp.17A319,17A319-3, May 2013

[11] Y. Liu, S.K. Kashif, A.M. Sohail, ”Engineering considerations on additional iron losses due to rotational fields and sheet cutting,” *Proc. of ICEM 2008*, 2008.

[12] P. Hargreaves, B.C. Mecrow, R. Hall, ”Calculation of iron loss in electrical generators using finite element analysis,” *Proc. of IEMDC 2011*, pp. 1368,1373, 2011

[13] [online] *http://www.iem.rwth-aachen.de*

[14] G. Müller, ”Berechnung elekrischer Maschinen”, Wiley-VCH: June 1996

[15] H. Dubbel, ”DUBBEL - Handbook of Mechanical Engineering”, Springer: October 1994

[16] [online] *http://medias.schaeffler.de/medias/en*

[17] Y. Takahashi, S. Wakao, M. Kondo, N. Terauchi, ”Loss analysis of permanent-magnet synchronous motor using three-dimensional finite-element method with homogenization method,” Journal of Applied Physics , vol.103, no.7, pp.07F126,07F126-3, Apr 2008

[18] D. Miyagi, N. Maeda, Y. Ozeki, K. Miki, N. Takahashi, “Estimation of Iron Loss in Motor Core With Shrink Fitting Using FEM Analysis,” *IEEE Trans. on Magn.*, vol. 45, no. 3, pp. 1704–1707, March 2009.

[19] Y. Oda, H. Toda, N. Shiga, S. Kasai, T. Hiratani, “Effect of Si Content on Iron Loss of Electrical Steel Sheet Under Compressive Stress,” *IEEE Trans. on Magn.*, vol. 50, no. 4, pp. 1–4, April 2014.

[20] K. Yamazaki, Y. Kato, “Iron Loss Analysis of Interior Permanent Magnet Synchronous Motors by Considering Mechanical Stress and Deformation of Stators and Rotors,” *IEEE Trans. on Magn.*, vol. 50, no. 2, pp. 909–912, Feb. 2014.

[21] D. Miyagi, K. Miki, M. Nakano, N. Takahashi, “Influence of Compressive Stress on Magnetic Properties of Laminated Electrical Steel Sheets,” *IEEE Trans. on Magn.*, vol. 46, no. 2, pp. 318–321, Feb. 2010.